VLSI Implementation of a Pipelined 128 points 4-Parallel radix-2³ FFT Architecture via Folding Transformation

James J. W. Kunst

`jjwk89@gmail.com`

Kevin H. Viglianco

`kevinvig7@gmail.com`

Daniel R. Garcia

`dani6rg@gmail.com`

Digital Signal Processing in Very Large Scale Integration Systems

Autumn 2019

Dr. Keshab K. Parhi
Dr. Ariel L. Pola

Universidad Nacional de Córdoba - FCEFyN
Av.Vélez Sársfield 1611, X5016GCA, Córdoba, Argentina

Fundación FULGOR
Ernesto Romagosa 518, Colinas V. Sarsfield, X5016GQN, Córdoba, Argentina

Abstract—- In this work we present a develop and VLSI implementation of a 4-parallel pipelined architecture for the complex fast Fourier transform (CFFT) based on the radix-2³ algorithm with 128 points using folding transformation and register minimization techniques. In addition, we are going to generate different synthesis levels from the hardware language description (HDL) with the purpose of obtaining a suitable performance on speed and area using standard cells at 45nm.

I. INTRODUCTION

The Fast Fourier Transform (FFT) is widely used in different applications' fields, particularly, it is used in algorithms that involves apply digital signal processing, e.g., calculate the Discrete Fourier Transform (DFT) efficiently, that is useful because in some applications is most convenient to work in frequency domain than time domain. Nowadays is common utilize the algorithm of FFT for real time applications and parallel-pipelined hardware architecture give us the opportunity to work at hight throughput rates.

There are two main types of pipelined FFT architectures [1]. On the one hand, feedback architectures (FB) which can be divided into Single-path Delay Feedback (SDF) and Multi-path Delay Feedback (MDF), theses methods take out samples from each butterflies stages and feed back to the registers or memories at the same stage. On the other hand, feedforward architectures such as Multi-Path Delay Commutator (MDC) where the main difference with the feedback architectures is that SDF transfer data samples from one stage to other stage

serially, instead of that the MDC architecture transfer more than one sample per clock cycle and do not have feedback loops.

We work focuses on the design of 4-parallel pipelined architecture radix-2³ 128-points for Complex FFT-DIF (Decimation in frequency). First, we will obtain the equations that correspond to Butterfly structure of *radix*-2³ FFT-DIF for 8 points. After that, we apply these idea to design a 2-parallel pipelined architecture radix-2³ 16-points FFT via folding transformation and find the appropriates rotators (*twiddle factors*) for each stage and clock cycle over the chain of butterflies on a feedforward architecture MDC. Second, we elaborate a float-point simulator which will process a summation of two cosine signals with different frequencies. Later, for the input and output of each stage of DFT, we quantized all operations such as adders and multipliers to get a fixed-point model. In this way, we can compare both models verifying the Signal to quantization noise ratio (SQNR) between fixed and float models.

Furthermore, we take the fixed-point model to elaborate our Synthesizable Verilog code HDL and verify the DFT functionality in each stage of the architecture. In addition to this, we generates power-area-timing report with different optimizations such as varying pipelining levels and canonical signed digit (CSD) to get a work frequency of $500Mhz$.

II. THE RADIX-2³ FFT ALGORITHM

The N-point DFT of an input sequence $x[n]$ is defined as:

$$X[k] = \sum_{n=0}^{N-1} x[n] \cdot W_N^{nk}, \quad k = 0, 1, ..., N-1 \qquad (1)$$

where $W_N^{nk} = e^{-j\frac{2\pi}{N}nk}$.

The FFT based on Cooley-Tukey algorithm is most commonly used in order to compute the DFT efficiently, this allows us reduce the number of operations from $O(N^2)$ for the DFT to $O(Nlog_2 N)$ for the FFT. Direct computation of the DFT is basically inefficient primarily because it does not exploit the symmetry and periodicity properties of the phase factor W_N, these two properties are:

$$\text{Symmetry property: } W_N^{k+N/2} = -W_N^k \qquad (2)$$

$$\text{Periodicity property: } W_N^{k+N} = W_N^k \qquad (3)$$

The development of computationally efficient algorithms for DFT is possible if we adopt a *Divide and Conquer* approach. This approach is based on the decomposition of an N point DFT into successively smaller DFTs. In accordance with this, the DFT is calculated in series of $s = log_\rho N$ stages, where ρ is the base of the *radix*. In our work this factor is two because we need to design a radix-2^3 FFT and this kind of radix is built using as principal base *radix-2*.

There are two methods to design FFT algorithms [2], [3]:

First, applying decimation in time (DIT), this results in a split of the N-point data sequence $x[n]$ into two $N/2$-point data sequences. Thus, we can obtain two different functions by decimating $x[n]$ by a factor of 2. The decimation of the data sequence can be repeated again and again until the resulting sequences are reduced to one-point sequence. In each decomposition, the basic computing unit that processes the samples is called *butterfly*.

Second, the decimation in frequency algorithm, is obtained by using the divide-and-conquer approach. To derive the algorithm we begin by splitting de DFT formula into two summations, one of which involves the sum over the first $N/2$ data points and the second sum involves the last $N/2$ data points

In general, each butterfly involves one complex multiplication and two complex additions. The main difference that we can see in Fig.1 between DIT and DIF is the instant in which the multiplication by W_N^ϕ is accomplished, it means, the input samples can be multiplied before or after of split and add internally the samples inside the butterfly structure.
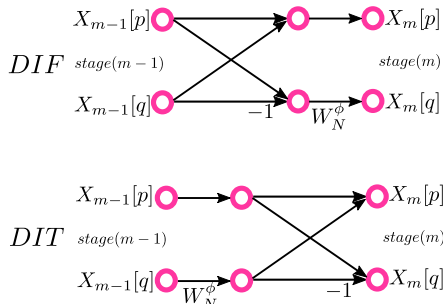

Figure 1: Basic butterflies computation in the decimation in time and frequency.

In addition, the input samples in FFT algorithms DIF are organized in natural order but its output has not in order, in this case is necessary a circuit for reordering the output data. On the other hand, FFT algorithms DIT is all the opposite, It has not its input in order and its output has a natural order.

Fallowing the methodology presented in [2], we can understand and apply the mathematical expressions of *radix-2^3* DIF explained in [4].

These fundamental equations are:

$$C_{8k+0} = \sum_{n=0}^{N/8-1} \left\{ [(x_n + x_{n+\frac{N}{2}}) + (x_{n+\frac{N}{4}} + x_{n+\frac{3N}{4}})] + \qquad (4) \right.$$
$$\left. [(x_{n+\frac{N}{8}} + x_{n+\frac{5N}{8}}) + (x_{n+\frac{3N}{8}} + x_{n+\frac{7N}{8}})] \right\} W_N^{0n} W_{N/8}^{nk}$$

$$C_{8k+4} = \sum_{n=0}^{N/8-1} \left\{ [(x_n + x_{n+\frac{N}{2}}) + (x_{n+\frac{N}{4}} + x_{n+\frac{3N}{4}})] - \right.$$
$$\left. [(x_{n+\frac{N}{8}} + x_{n+\frac{5N}{8}}) + (x_{n+\frac{3N}{8}} + x_{n+\frac{7N}{8}})] \right\} W_N^{4n} W_{N/8}^{nk}$$

$$C_{8k+2} = \sum_{n=0}^{N/8-1} \left\{ [(x_n + x_{n+\frac{N}{2}}) - (x_{n+\frac{N}{4}} + x_{n+\frac{3N}{4}})] - j \right.$$
$$\left. [(x_{n+\frac{N}{8}} + x_{n+\frac{5N}{8}}) - (x_{n+\frac{3N}{8}} + x_{n+\frac{7N}{8}})] \right\} W_N^{2n} W_{N/8}^{nk}$$

$$C_{8k+6} = \sum_{n=0}^{N/8-1} \left\{ [(x_n + x_{n+\frac{N}{2}}) - (x_{n+\frac{N}{4}} + x_{n+\frac{3N}{4}})] + j \right.$$
$$\left. [(x_{n+\frac{N}{8}} + x_{n+\frac{5N}{8}}) - (x_{n+\frac{3N}{8}} + x_{n+\frac{7N}{8}})] \right\} W_N^{6n} W_{N/8}^{nk}$$

$$C_{8k+1} = \sum_{n=0}^{N/8-1} \left\{ [(x_n - x_{n+\frac{N}{2}}) - j(x_{n+\frac{N}{4}} - x_{n+\frac{3N}{4}})] + W_N^{N/8} \right.$$
$$\left. [(x_{n+\frac{N}{8}} - x_{n+\frac{5N}{8}}) - j(x_{n+\frac{3N}{8}} - x_{n+\frac{7N}{8}})] \right\} W_N^n W_{N/8}^{nk}$$

$$C_{8k+5} = \sum_{n=0}^{N/8-1} \left\{ [(x_n - x_{n+\frac{N}{2}}) - j(x_{n+\frac{N}{4}} - x_{n+\frac{3N}{4}})] - W_N^{N/8} \right.$$
$$\left. [(x_{n+\frac{N}{8}} - x_{n+\frac{5N}{8}}) - j(x_{n+\frac{3N}{8}} - x_{n+\frac{7N}{8}})] \right\} W_N^{5n} W_{N/8}^{nk}$$

$$C_{8k+3} = \sum_{n=0}^{N/8-1} \left\{ [(x_n - x_{n+\frac{N}{2}}) + j(x_{n+\frac{N}{4}} - x_{n+\frac{3N}{4}})] + W_N^{3N/8} \right.$$
$$\left. [(x_{n+\frac{N}{8}} - x_{n+\frac{5N}{8}}) + j(x_{n+\frac{3N}{8}} - x_{n+\frac{7N}{8}})] \right\} W_N^{3n} W_{N/8}^{nk}$$

$$C_{8k+7} = \sum_{n=0}^{N/8-1} \left\{ [(x_n - x_{n+\frac{N}{2}}) + j(x_{n+\frac{N}{4}} + x_{n+\frac{3N}{4}})] - W_N^{3N/8} \right.$$
$$\left. [(x_{n+\frac{N}{8}} - x_{n+\frac{5N}{8}}) + j(x_{n+\frac{3N}{8}} - x_{n+\frac{7N}{8}})] \right\} W_N^{7n} W_{N/8}^{nk}$$

In Fig. 2 and Fig. 3 we represent the equivalent diagram of interconnections and data flows from the equations presented in (4).

The use of higher value radices lead to different amount of rotators. If we compare the quantity of rotators of an architecture *radix-2* FFT with an architecture *radix-2^k* FFT, this last has less number of phase factors than use a *radix-2*.

With these first approaches, we are in conditions to design a 128-*points* DFT *radix-2^3*. Applying the divide and conquer
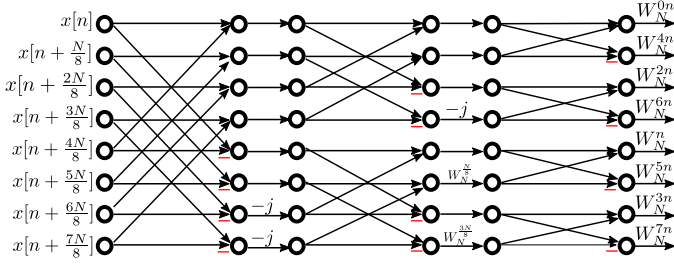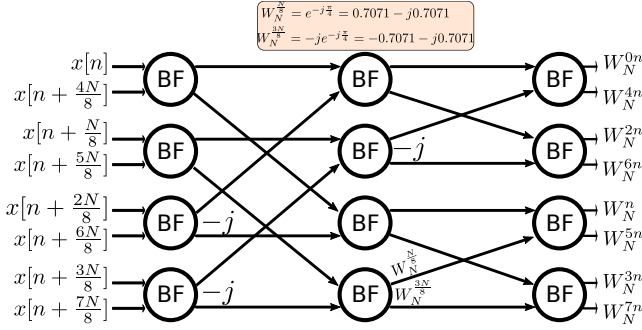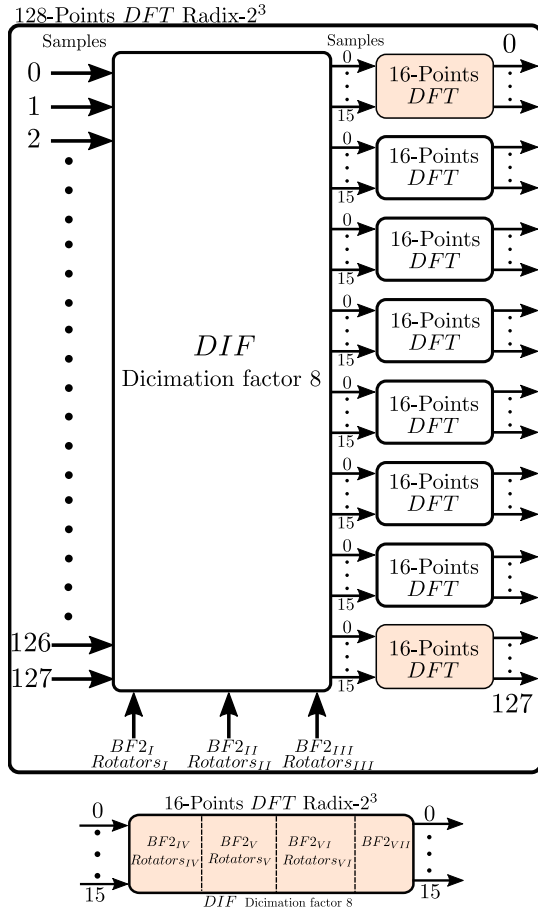
Figure 2: Structure of interconnection for *radix*-2^3 DIF DFT

Figure 3: Data flow graph (DFG) based in equations (4).

Figure 4: Decomposing a *radix*-2^3 128-point DFT

$\sum_{n=0}^{128/8-1}\{\cdot\}$, for $k = 0, 1, ..., (128/8) - 1$. In this way we get a sequence in chain of butterflies with its corresponding rotation factor and the correct index of the samples in witch them must be added or multiplied. This technique lets us do a subdivision on butterflies' stages, in Fig. 4 we can see that the 128 point DFT goes through a processes that involve tree stages of butterflies to arrive finally to a set of eight DFT where each of one is a 16 point DFT.

The next step to can calculate finally our 128 point DFT is to find the suitable rotator factors for the 16 point DFT, this process follow exactly the same calculation that we comment and remark previously, the use of the above equations (4) are essential for this design and them are evaluated to get $C_{8k+i} = \sum_{n=0}^{16/8-1}\{\cdot\}$, for $k = 0, 1$. The structure for the 16 point DFT is described in Fig. 5 and Fig. 6.
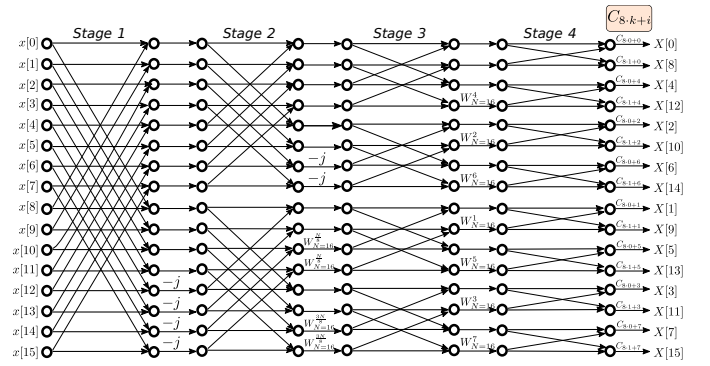
Figure 5: Flow graph of a *radix*-2^3 16-point DIF DFT
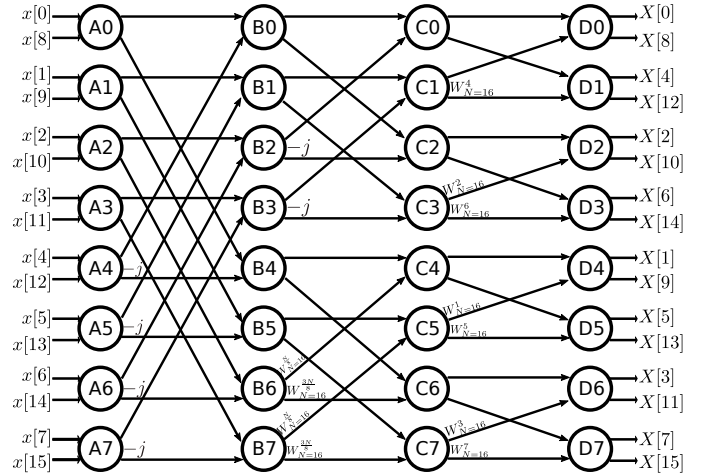
Figure 6: Data flow graph (DFG) for a *radix*-2^3 16-point DIF DFT

With the DFT's previous decomposition we learned how to get whole the coefficients C_{8k+i} that represent the samples in frequency $X[k]$ obtained from a combination of the different instances of $x[n]$. This method take us to apply step by step the equation (4) to our design and finally arrive to the definitive architecture, the Fig. 7 shows us a *radix*-2^3 128-point DIF DFT with a total of seven stages where each stage is building with 64 butterflies of radix-2 base.
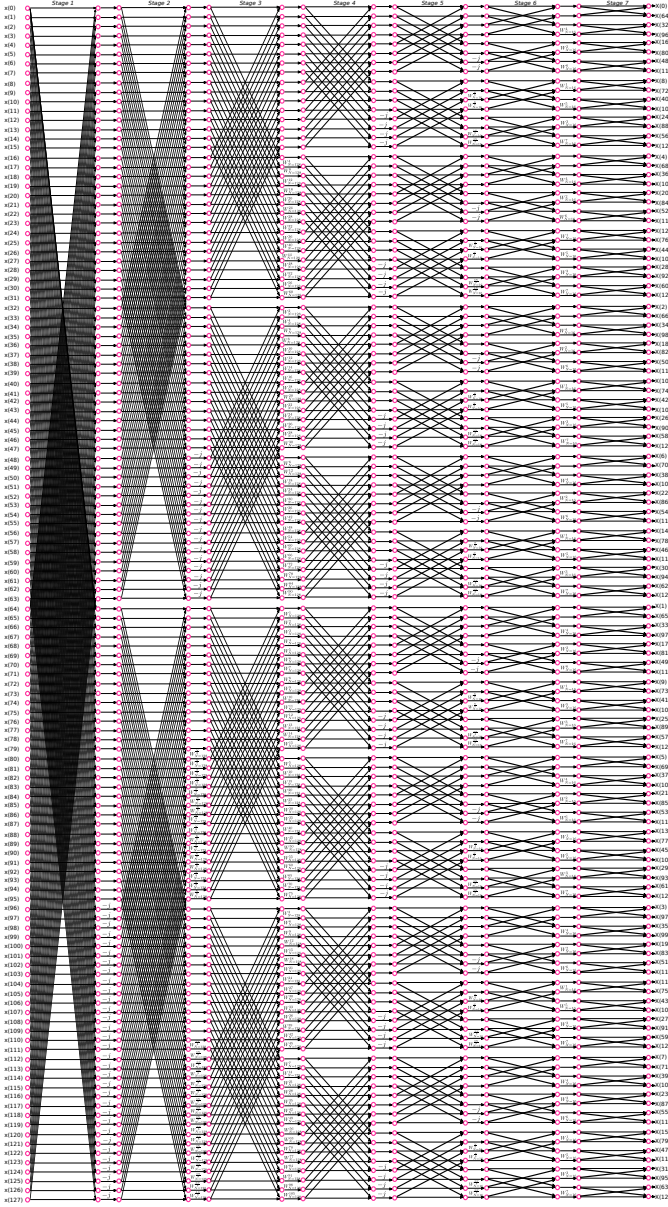
strategy by decomposition of a 128-point DFT in smaller DFTs. We begin to apply the set of equations (4) for the 128 point DFT and calculating each coefficient $C_{8k+i} =$

Figure 7: Flow graph of a *radix*-2^3 128-point DIF DFT

III. DESIGN OF FFT ARCHITECTURE VIA FOLDING

In this section, we illustrate the folding transformation method to derive a 16-point DIF FFT 4-parallel architecture as an example and then, using the same method, we extend it to 128-point architecture. To do this, we will use the architecture proposed in [5].

A. 4-Parallel radix-2^3 16-Points

In Fig. 5 we can see the flow graph of a 16-point DIF FFT radix-2^3 with main base radix-2. The graph is divided into four stages and each of them consist of a set of butterflies and multipliers. The twiddle factor in between the stages indicates a multiplication by W_N^k, where W_N denotes the Nth root of unity, with its exponent evaluated modulo N. This can be represented as a DFG as shown in Fig. 6 where the

nodes represents the butterfly computations of the radix-2 FFT algorithm.

The folding transformation is used on the DFG in to derive a pipelined architecture. To do this we need a folding set, which is an ordered set of operations executed by the same functional unit. Each folding set contains K entries, where K is called the folding factor. The operation in the jth position within the folding set (where goes from 0 to K-1) is executed by the functional unit during the time partition. The term is called the folding order.

First we need to derive the folding equations, to do this consider an edge e connecting the nodes U and V with $w(e)$ delays. Let the executions of the lth iteration of the nodes U and V be scheduled at the time units $Kl + u$ and $Kl + v$ respectively, where u and v are the folding orders of the nodes U and V, respectively. The folding equation for the edge e is:

$$D_F(U \rightarrow V) = Kw(e) - P_U + v - u \qquad (5)$$

where P_U is the number of pipeline stages in the hardware unit which executes the node U. Consider folding of the the DFG in Fig. 6 with the folding sets:

$$A = \{A0, A2, A4, A6\} \qquad A' = \{A1, A3, A5, A7\}$$
$$B = \{B1, B3, B0, B2\} \qquad B' = \{B5, B7, B4, B6\}$$
$$C = \{C2, C1, C3, C0\} \qquad C' = \{C6, C5, C7, C4\}$$
$$D = \{D3, D0, D2, D1\} \qquad D' = \{D7, D4, D6, D5\}$$

Assuming that the butterfly operations do not have any pipeline stages ($P_A = P_B = P_C = P_D = 0$), the folding equations can be derived for all edges. Thus, we can obtained from (5) the expressions *without apply retiming*.

$$D_F(D0 \rightarrow B0) = 2 \qquad D_F(D0 \rightarrow B4) = 2$$
$$D_F(D1 \rightarrow B1) = 0 \qquad D_F(D1 \rightarrow B5) = 0$$
$$D_F(D2 \rightarrow B2) = 2 \qquad D_F(D2 \rightarrow B6) = 2$$
$$D_F(D3 \rightarrow B3) = -1 \qquad D_F(D3 \rightarrow B7) = -1$$
$$D_F(D4 \rightarrow B0) = 0 \qquad D_F(D4 \rightarrow B4) = 0$$
$$D_F(D5 \rightarrow B1) = -1 \qquad D_F(D5 \rightarrow B5) = -1$$
$$D_F(D6 \rightarrow B2) = 0 \qquad D_F(D6 \rightarrow B6) = 0$$
$$D_F(D7 \rightarrow B3) = -2 \qquad D_F(D7 \rightarrow B7) = -2$$
$$D_F(E0 \rightarrow C0) = 1 \qquad D_F(E0 \rightarrow C2) = -2$$
$$D_F(E1 \rightarrow C1) = 1 \qquad D_F(E1 \rightarrow C3) = 2$$
$$D_F(E2 \rightarrow C0) = 0 \qquad D_F(E2 \rightarrow C2) = -3$$
$$D_F(E3 \rightarrow C1) = 0 \qquad D_F(E3 \rightarrow C3) = 1$$
$$D_F(E4 \rightarrow C4) = 1 \qquad D_F(E4 \rightarrow C6) = -2$$
$$D_F(E5 \rightarrow C5) = 1 \qquad D_F(E5 \rightarrow C7) = 2$$
$$D_F(E6 \rightarrow C4) = 0 \qquad D_F(E6 \rightarrow C6) = -3$$
$$D_F(E7 \rightarrow C5) = 0 \qquad D_F(E7 \rightarrow C7) = 1$$
$$D_F(F0 \rightarrow D0) = -2 \qquad D_F(F0 \rightarrow D1) = 0$$
$$D_F(F1 \rightarrow D0) = 0 \qquad D_F(F1 \rightarrow D1) = 2$$
$$D_F(F2 \rightarrow D2) = 2 \qquad D_F(F2 \rightarrow D3) = 0$$
$$D_F(F3 \rightarrow D2) = 0 \qquad D_F(F3 \rightarrow D3) = -2$$
$$D_F(F4 \rightarrow D4) = -2 \qquad D_F(F4 \rightarrow D5) = 0$$
$$D_F(F5 \rightarrow D4) = 0 \qquad D_F(F5 \rightarrow D5) = 2$$
$$D_F(F6 \rightarrow D6) = 2 \qquad D_F(F6 \rightarrow D7) = 0$$
$$D_F(F7 \rightarrow D6) = 0 \qquad D_F(F7 \rightarrow D7) = -2$$

For the folded system to be realizable, $D_F(U \rightarrow V) \geq 0$ must hold for all the edges in the DFG. Retiming and/or pipeline can be applied to satisfy this property, if the DFG in Fig. 6 is pipelined/retimmed as shown in Fig. 8 the system is realizable and the folded delays for the edges are given by the equations that represent a folding set *with retiming*
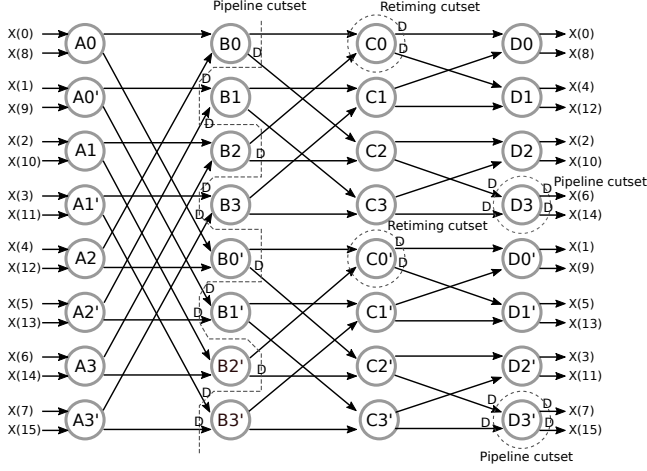

Figure 8: Data Flow graph (DFG) of a radix-2 16-point DIF FFT with retiming and pipeline.

$$D_F(D0 \rightarrow B0) = 2 \qquad D_F(D0 \rightarrow B4) = 2 \qquad (6)$$
$$D_F(D1 \rightarrow B1) = 4 \qquad D_F(D1 \rightarrow B5) = 4$$
$$D_F(D2 \rightarrow B2) = 2 \qquad D_F(D2 \rightarrow B6) = 2$$
$$D_F(D3 \rightarrow B3) = 3 \qquad D_F(D3 \rightarrow B7) = 3$$
$$D_F(D4 \rightarrow B0) = 0 \qquad D_F(D4 \rightarrow B4) = 0$$
$$D_F(D5 \rightarrow B1) = 3 \qquad D_F(D5 \rightarrow B5) = 3$$
$$D_F(D6 \rightarrow B2) = 0 \qquad D_F(D6 \rightarrow B6) = 0$$
$$D_F(D7 \rightarrow B3) = 2 \qquad D_F(D7 \rightarrow B7) = 2$$
$$D_F(E0 \rightarrow C0) = 1 \qquad D_F(E0 \rightarrow C2) = 2$$
$$D_F(E1 \rightarrow C1) = 1 \qquad D_F(E1 \rightarrow C3) = 2$$
$$D_F(E2 \rightarrow C0) = 0 \qquad D_F(E2 \rightarrow C2) = 1$$
$$D_F(E3 \rightarrow C1) = 0 \qquad D_F(E3 \rightarrow C3) = 1$$
$$D_F(E4 \rightarrow C4) = 1 \qquad D_F(E4 \rightarrow C6) = 2$$
$$D_F(E5 \rightarrow C5) = 1 \qquad D_F(E5 \rightarrow C7) = 2$$
$$D_F(E6 \rightarrow C4) = 0 \qquad D_F(E6 \rightarrow C6) = 1$$
$$D_F(E7 \rightarrow C5) = 0 \qquad D_F(E7 \rightarrow C7) = 1$$
$$D_F(F0 \rightarrow D0) = 2 \qquad D_F(F0 \rightarrow D1) = 4$$
$$D_F(F1 \rightarrow D0) = 0 \qquad D_F(F1 \rightarrow D1) = 2$$
$$D_F(F2 \rightarrow D2) = 2 \qquad D_F(F2 \rightarrow D3) = 4$$
$$D_F(F3 \rightarrow D2) = 0 \qquad D_F(F3 \rightarrow D3) = 2$$
$$D_F(F4 \rightarrow D4) = 2 \qquad D_F(F4 \rightarrow D5) = 4$$
$$D_F(F5 \rightarrow D4) = 0 \qquad D_F(F5 \rightarrow D5) = 2$$
$$D_F(F6 \rightarrow D6) = 2 \qquad D_F(F6 \rightarrow D7) = 4$$
$$D_F(F7 \rightarrow D6) = 0 \qquad D_F(F7 \rightarrow D7) = 2$$

We can see that the number of register required to implement the folding equations in (6) is 80. For minimize the number of registers we use the register minimization technique. If we let the output of node A1 be $y_{(0)}$ and $y_{(8)}$, applying this successively with the rest of the nodes A we can obtain the linear life time chart for this stage in Fig. 9. Applying this
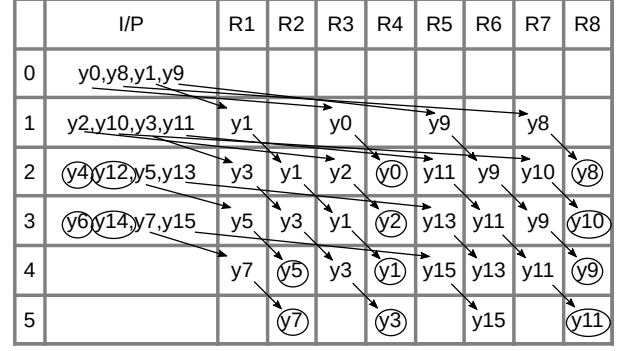
	I/P	R1	R2	R3	R4	R5	R6	R7	R8
0	y0,y8,y1,y9								
1	y2,y10,y3,y11	y1		y0		y9		y8	
2	y4,y12,y5,y13	y3	y1	y2	y0	y11	y9	y10	y8
3	y6,y14,y7,y15	y5	y3	y1	y2	y13	y11	y9	y10
4		y7	y5	y3	y1	y15	y13	y11	y9
5			y7		y3		y15		y11

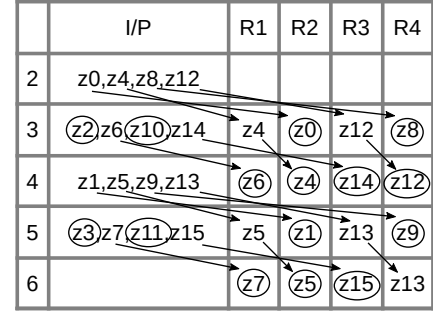Figure 9: Linear lifetime chart for the variables $y_{(0)}, y_{(1)}, ..., y_{(15)}$ for a 16-point FFT architecture.

	I/P	R1	R2	R3	R4
2	z0,z4,z8,z12				
3	z2,z6,z10,z14	z4	z0	z12	z8
4	z1,z5,z9,z13	z6	z4	z14	z12
5	z3,z7,z11,z15	z5	z1	z13	z9
6		z7	z5	z15	z13

Figure 10: Linear lifetime chart for the variables $z_{(0)}, z_{(1)}, ..., z_{(15)}$ for a 16-point FFT architecture.

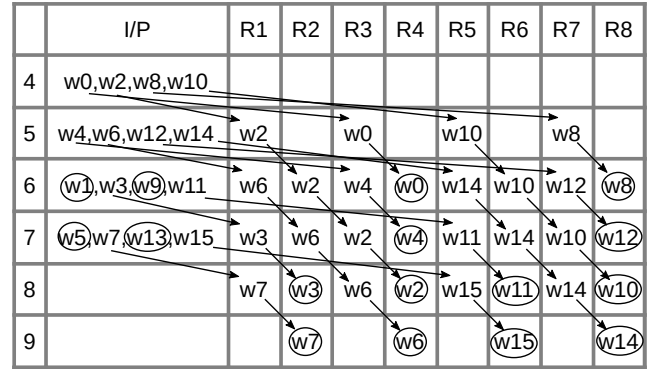|	I/P	R1	R2	R3	R4	R5	R6	R7	R8
4	w0,w2,w8,w10								
5	w4,w6,w12,w14	w2		w0		w10		w8	
6	w1,w3,w9,w11	w6	w2	w4	w0	w14	w10	w12	w8
7	w5,w7,w13,w15	w3	w6	w2	w4	w11	w14	w10	w12
8		w7	w3	w6	w2	w15	w11	w14	w10
9			w7		w6		w15		w14

Figure 11: Linear lifetime chart for the variables $w_{(0)}, w_{(1)}, ..., w_{(15)}$ for a 16-point FFT architecture.

criteria to the rest of the stages we can obtain the life time chart 10 and 11 for the outputs of the nodes B and C respectively, we can see that the numbers of maximum registers in each stage are 8, 4 and 8 respectively. More information about this method can be found on [6]. The register allocation tables for each of lifetime charts are shown in Fig. 12, 13 and 14 respectively, we can implement the same equations in (6) using 20 registers with register minimization techniques. The folded architecture in Fig. 17 is synthesized using the folding equations and the register allocation tables, the method can be found in [6].

The inputs of each folding node are represented with a matrix where the values in the same column are data that flow in parallel and values in the same row flow through the same
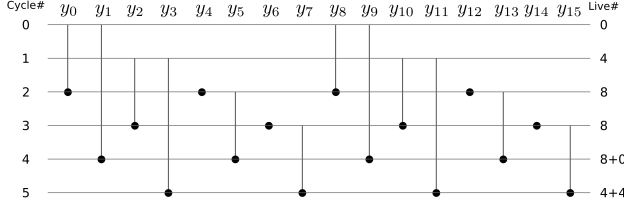
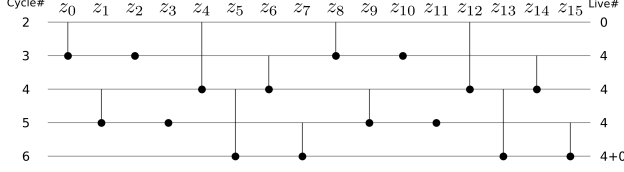Figure 12: Register allocation table for the data represented in 9

Figure 13: Register allocation table for the data represented in 10
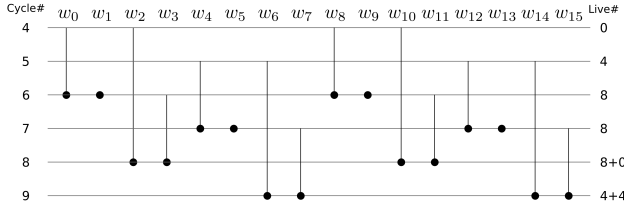

Figure 14: Register allocation table for the data represented in 11

path in consecutive clock cycles. The first two rows represents the inputs of the superior BF and the others two represents the input of the inferior BF. The same criteria is used for represent the constants of rotators, where each number k of the matrix represent a multiplication by W_N^k. As we can see in Fig. 17, we suppose that the inputs and output are not ordered, to order these variables extra logic are needed, using more registers and multiplexers.

The different types of rotators used in Fig. 17 are shown in Fig. 15, the description of each of them can be found below.

- Trivial rotator: They can be carried out by interchanging the real and imaginary components and/or changing the sign of the data.
- Constant CSD rotator: They can be carried out by interchanging the real and imaginary components and/or a multiplication by a unique constant fractional number, in this case we will use a CSD multiplier to perform the area utilized.
- General rotator: They can be carried out by interchanging the real and imaginary components and/or a multiplication by more than one constant fractional numbers, in this case we will use a general multiplier.
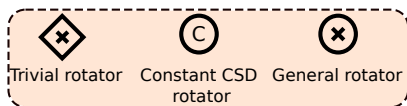

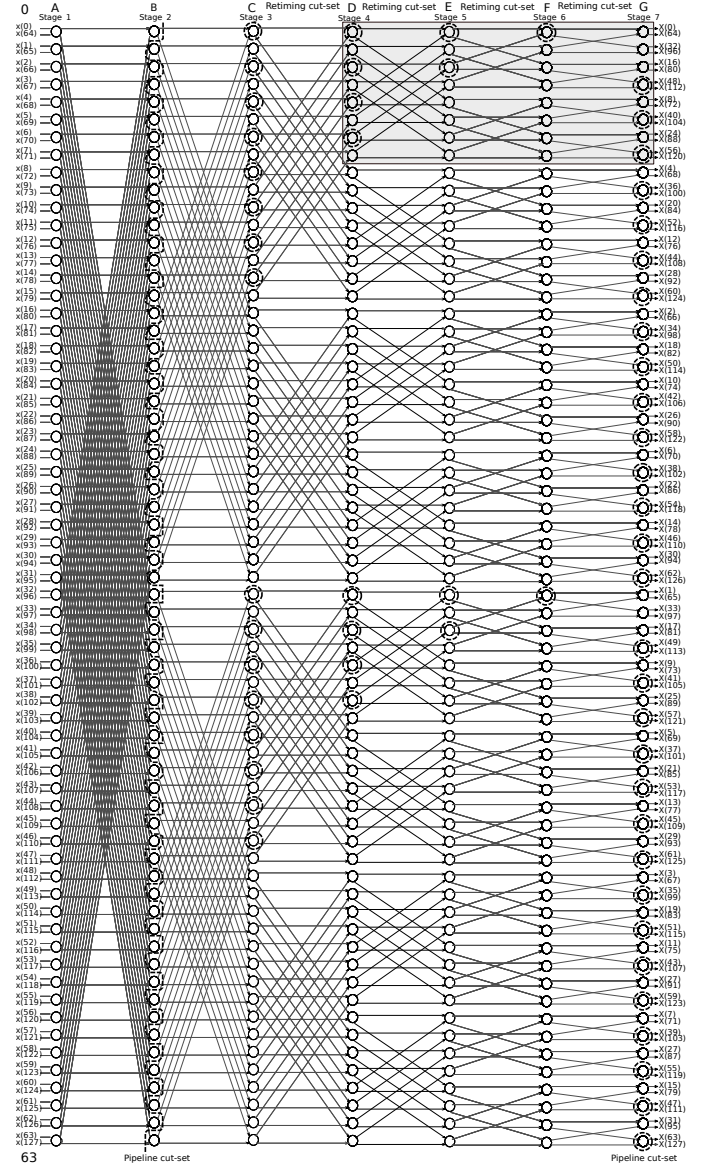Figure 15: Symbols used for the different types of rotators

Figure 16: Pipelined DFG of a 128-point DIF FFT as a preprocessing step for folding.

B. 4-Parallel radix-2^3 128-Points

We can deduce the folding architecture following the same method than used with the 4-Parallel radix-2^3 16-Points. The DFG and folding set used can be shown in Fig. 16 and Table I. The architecture can be seen in Fig. 18.

IV. IMPLEMENTATION

In this section we are going to begin with the process of how accomplish the implementation of our 4-parallel architecture for the computation of 128-point *radix*-2^3 DIF complex FFT. First, we wrote a *MATLAB* simulator to validate the operation of our design and the design presented in [7], [8]. Therefore, we can have a reference architecture for compare the design that we deduce. After that, we take all these information to generate a Synthesizable *Verilog* code with different levels of optimizations with a powerful tool like *Synopsys* to get a final design integrated of Standard Cells @45*nm*.
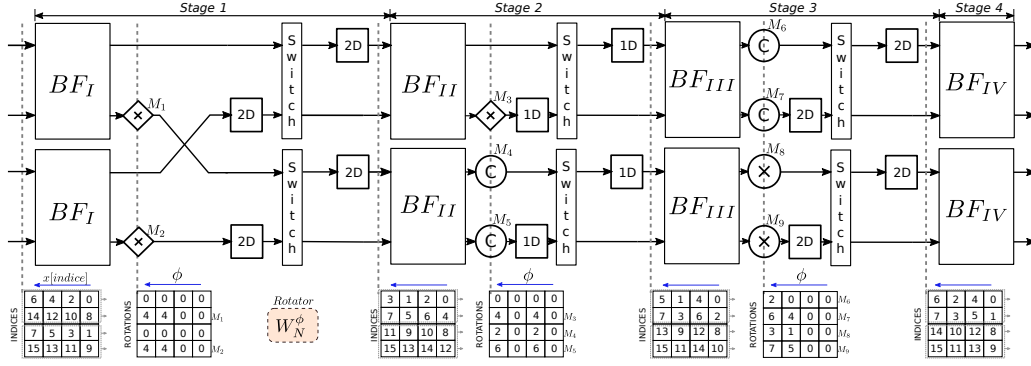
Figure 17: Folding architecture for the computation of a radix-2^3 16-point DIF complex FFT.

Table I: Folding set for the DFG showed in Fig. 16

|																
A	A0	A2	A4	A6	A8	A10	A12	A14	A16	A18	A20	A22	A24	A26	A28	A30
	A32	A34	A36	A38	A40	A42	A44	A46	A48	A50	A52	A54	A56	A58	A60	A62
A'	A1	A3	A5	A7	A9	A11	A13	A15	A17	A19	A21	A23	A25	A27	A29	A31
	A33	A35	A37	A39	A41	A43	A45	A47	A49	A51	A53	A55	A57	A59	A61	A63
B	B1	B3	B5	B7	B9	B11	B13	B15	B17	B19	B21	B23	B25	B27	B29	B31
	B0	B2	B4	B6	B8	B10	B12	B14	B16	B18	B20	B22	B24	B26	B28	B30
B'	B33	B35	B37	B39	B41	B43	B45	B47	B49	B51	B53	B55	B57	B59	B61	B63
	B32	B34	B36	B38	B40	B42	B44	B46	B48	B50	B52	B54	B56	B58	B60	B62
C	C16	C18	C20	C22	C24	C26	C28	C30	C1	C3	C5	C7	C9	C11	C13	C15
	C17	C19	C21	C23	C25	C27	C29	C31	C0	C2	C4	C6	C8	C10	C12	C14
C'	C48	C50	C52	C54	C56	C58	C60	C62	C33	C35	C37	C39	C41	C43	C45	C47
	C49	C51	C53	C55	C57	C59	C61	C63	C32	C34	C36	C38	C40	C42	C44	C46
D	D8	D10	D12	D14	D16	D18	D20	D22	D24	D26	D28	D30	D1	D3	D5	D7
	D9	D11	D13	D15	D17	D19	D21	D23	D25	D27	D29	D31	D0	D2	D4	D6
D'	D40	D42	D44	D46	D48	D50	D52	D54	D56	D58	D60	D62	D33	D35	D37	D39
	D41	D43	D45	D47	D49	D51	D53	D55	D57	D59	D61	D63	D32	D34	D36	D38
E	E4	E6	E8	E10	E12	E14	E16	E18	E20	E22	E24	E26	E28	E30	E1	E3
	E5	E7	E9	E11	E13	E15	E17	E19	E21	E23	E25	E27	E29	E31	E0	E2
E'	E36	E38	E40	E42	E44	E46	E48	E50	E52	E54	E56	E58	E60	E62	E33	E35
	E37	E39	E41	E43	E45	E47	E49	E51	E53	E55	E57	E59	E61	E63	E32	E34
F	F2	F4	F6	F8	F10	F12	F14	F16	F18	F20	F22	F24	F26	F28	F30	F1
	F3	F5	F7	F9	F11	F13	F15	F17	F19	F21	F23	F25	F27	F29	F31	F0
F'	F34	F36	F38	F40	F42	F44	F46	F48	F50	F52	F54	F56	F58	F60	F62	F33
	F35	F37	F39	F41	F43	F45	F47	F49	F51	F53	F55	F57	F59	F61	F63	F32
G	G3	G5	G7	G9	G11	G13	G15	G17	G19	G21	G23	G25	G27	G29	G31	G0
	G2	G4	G6	G8	G10	G12	G14	G16	G18	G20	G22	G24	G26	G28	G30	G1
G'	G35	G37	G39	G41	G43	G45	G47	G49	G51	G53	G55	G57	G59	G61	G63	G32
	G34	G36	G38	G40	G42	G44	G46	G48	G50	G52	G54	G56	G58	G60	G62	G33
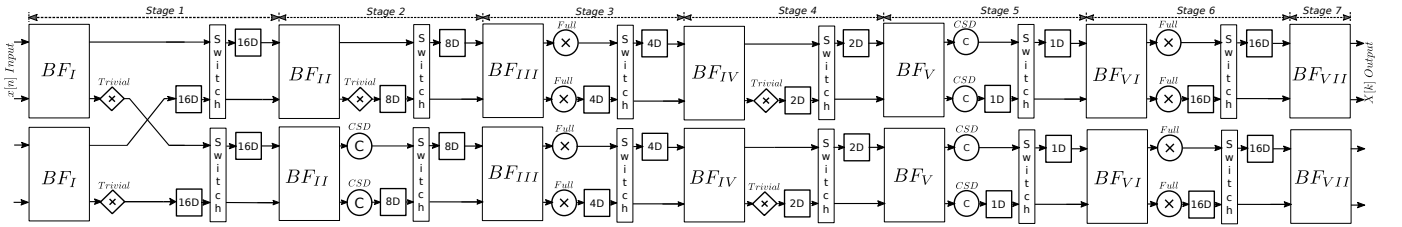
Figure 18: Folding architecture for the computation of a radix-2^3 128-point DIF complex FFT.

A. Floating and Fixed point Simulator

The input signal Fig. 20 to our architecture will be a mixture of sinusoid signals with two frequency values, theses signal will be normalizing to the unity and in this way we can have a test bench design.

$$x'[n] = cos(2\pi f_1 nT_s) + cos(2\pi f_2 nT_s) \qquad (7)$$
$$x[n] = x'[n]/max\{x'[n]\}$$

where $f_1 = 100Hz$, $f_2 = 1000Hz$ and T_s is the sampled period.

In each stage of the Fig. 19, input samples that propagate stage by stage will be carefully quantized with the purpose of getting a high SQNR (Signal to Quantization Noise Ratio).

$$SQNR_{dB} = 10log_{10}\left(\frac{Var\{Signal_{FloatPoint}\}}{Var\{Signal_{FloatPoint} - Signal_{FixedPoint}\}}\right)$$

SQNR represents computing the logarithmic relationship between float signal variance over error variance from an signal given.

The input signal $x[n]$ is quantized with a value of $S(10, 9)$, that representation means a number signed (S) with 10 total
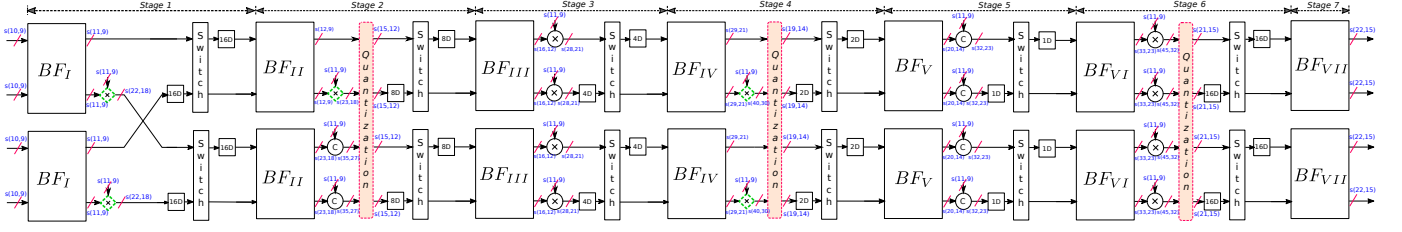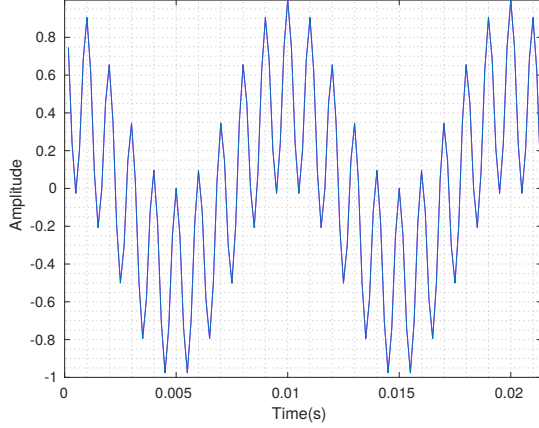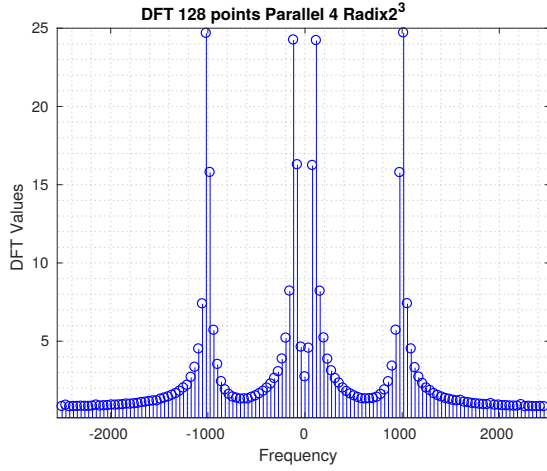
Figure 19: Quantization for a 128-point 4-parallel pipelined complex FFT architecture

Figure 20: Input signal $x[n]$ in time domain

Figure 21: Output samples, absolute value vs frequency $|X[k]|$

Figure 22: Circuit for data shuffling

Figure 23: Complex butterfly
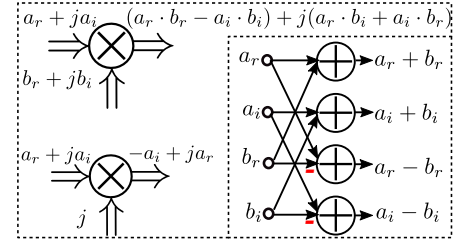
Figure 24: Complex multiplier and complex adder

bits and 9 fractional bits. The value calculated of SQNR for the input is $56.9dB$. Following the same steps, we can compute the SQNR for the *twiddle* factors and the architecture's output.

Twiddles factor are quantized with a relation of $S(11, 9)$ and the complex output signal $X[k]$ with $S(22, 15)$. Output quantization for the real part is $46.8dB$ and for the imaginary part $47.3dB$. In general, a value of quantization close to $50dB$ is a good approximation. Out signal from our *MATLAB* fixed-point model from the architecture in Fig. 19 the output signal is given in Fig. 21, that represents a first approach in our calculation of a DFT without optimization.

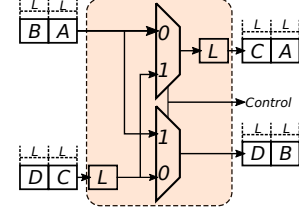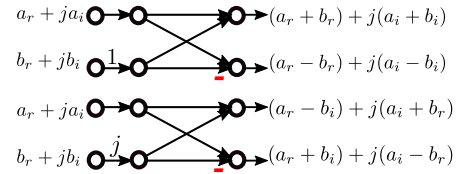The combination between latencies (delays registers) and switches in all stages in Fig. 19 is the equivalent circuit shows in Fig. 22, that is used to appropriately order samples in each butterflies input.

Whole elements on the architecture such as multipliers and butterflies are complex as Fig. 23 and 24. On an implementation is essential divide the signal in its real and imaginary part with the purpose of process them independently. A *general rotator* (full complex multiplier) generate a real and imaginary component that is composed by a real multiplication an one addition, but a *trivial rotator* only change the components of a complex signal. These relations are important at the moment of doing the quantization process to ensure an appropriate quantity of bits.
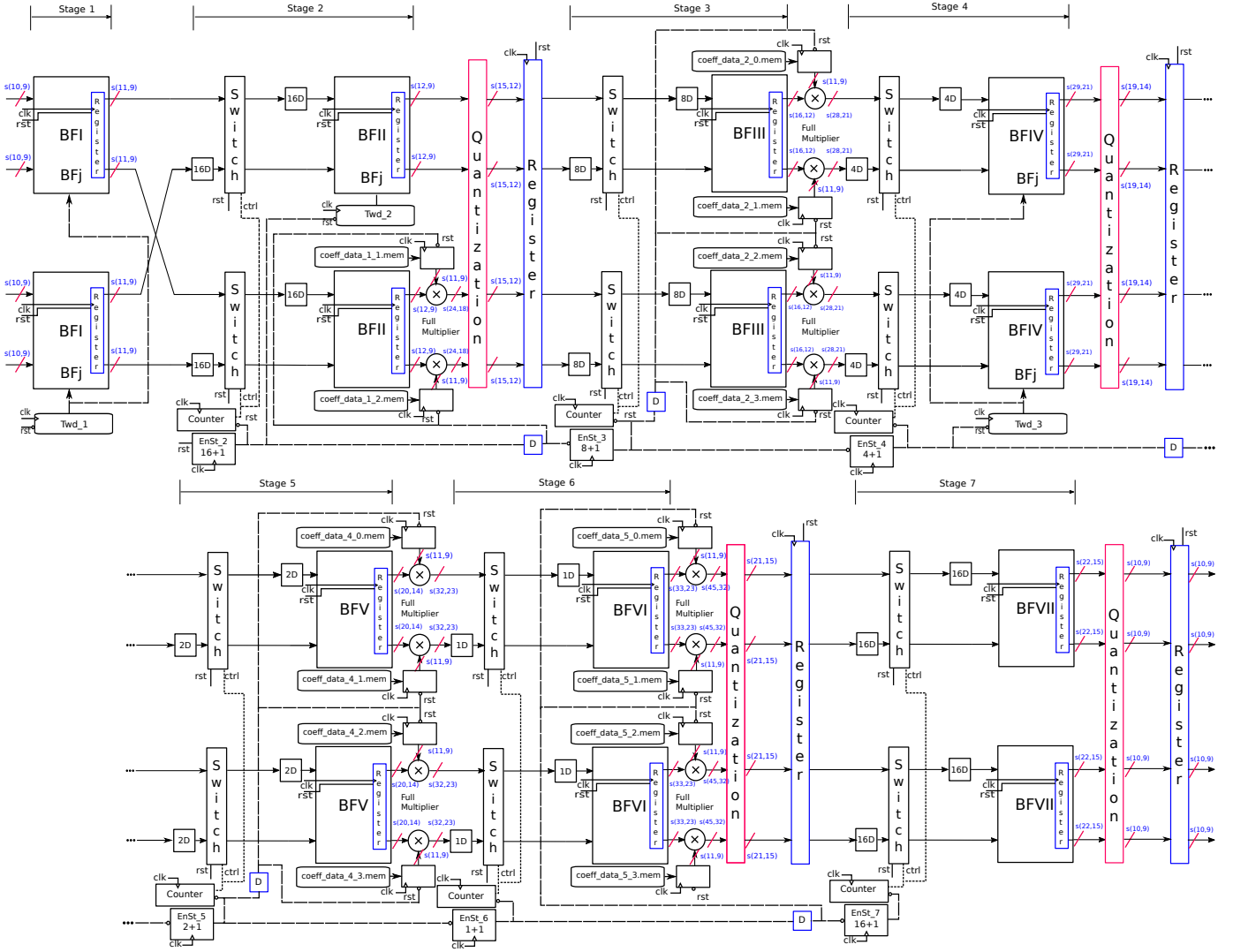
B. Verilog (HDL) Model

Hello wold!

Figure 25: RTL (Register transfer level) design for a 4-parallel *radix*-2^3 128-point DIF FFT with Optimization

V. RESULTS

VI. CONCLUSION

REFERENCES

[1] Shousheng He and M. Torkelson, "Designing pipeline FFT processor for OFDM (de)modulation," in *1998 URSI International Symposium on Signals, Systems, and Electronics. Conference Proceedings (Cat. No.98EX167)*. IEEE, pp. 257–262. [Online]. Available: http://ieeexplore.ieee.org/document/738077/

[2] J. G. Proakis and D. G. Manolakis, "DIGITAL SIGNAL PROCESSING," p. 1033.

[3] A. V. Oppenheim and R. W. Schafer, *Tratamiento de señales en tiempo discreto, tercera edición*. Pearson Educación, OCLC: 843859190.

[4] L. Jia, Y. Gao, and H. Tenhunen, "Efficient VLSI implementation of radix-8 FFT algorithm," p. 4.

[5] M. Ayinala, M. Brown, and K. K. Parhi, "Pipelined Parallel FFT Architectures via Folding Transformation," *IEEE Transactions on Very Large Scale Integration (VLSI) Systems*, vol. 20, no. 6, pp. 1068–1081, Jun. 2012. [Online]. Available: http://ieeexplore.ieee.org/document/5776727/

[6] K. K. Parhi, *VLSI Digital Signal Processing Systems. Design and implementation*. JOHN WILEY & SONS, INC., 1999, pp. 157–163.

[7] M. Garrido, J. Grajal, M. A. Sanchez, and O. Gustafsson, "Pipelined Radix-2^{k} Feedforward FFT Architectures," *IEEE Transactions on Very Large Scale Integration (VLSI) Systems*, vol. 21, no. 1, pp. 23–32, Jan. 2013. [Online]. Available: http://ieeexplore.ieee.org/document/6118316/

[8] M. Garrido, S.-J. Huang, and S.-G. Chen, "Feedforward FFT hardware architectures based on rotator allocation," vol. 65, no. 2, pp. 581–592. [Online]. Available: http://ieeexplore.ieee.org/document/8010853/